ADVANCES IN ATMOSPHERIC SCIENCES, VOL. 35, FEBRUARY 2018, 135–145

• **Original Paper** •

Can MODIS Detect Trends in Aerosol Optical Depth over Land?

Xuehua FAN*[1], Xiang'ao XIA[1,2,3], and Hongbin CHEN[1,2,3]

[1]*Key Laboratory of Middle Atmosphere and Global Environment Observation, Institute of Atmospheric Physics, Chinese Academy of Sciences, Beijing* 100029*, China*

[2]*School of the Earth Science, Chinese Academy of Science University, Beijing* 100049*, China*

[3]*Collaborative Innovation Center on Forecast and Evaluation of Meteorological Disasters, Nanjing University of Information Science and Technology, Nanjing* 210044*, China*

(Received 17 February 2017; revised 6 July 2017; accepted 11 July 2017)

ABSTRACT

The Moderate Resolution Imaging Spectroradiometer (MODIS) sensor onboard NASA's Aqua satellite has been collecting valuable data about the Earth system for more than 14 years, and one of the benefits of this is that it has made it possible to detect the long-term variation in aerosol loading across the globe. However, the long-term aerosol optical depth (AOD) trends derived from MODIS need careful validation and assessment, especially over land. Using AOD products with at least 70 months' worth of measurements collected during 2002–15 at 53 Aerosol Robotic Network (AERONET) sites over land, Mann–Kendall (MK) trends in AOD were derived and taken as the ground truth data for evaluating the corresponding results from MODIS onboard Aqua. The results showed that the AERONET AOD trends over all sites in Europe and North America, as well as most sites in Africa and Asia, can be reproduced by MODIS/Aqua. However, disagreement in AOD trends between MODIS and AERONET was found at a few sites in Australia and South America. The AOD trends calculated from AERONET instantaneous data at the MODIS overpass times were consistent with those from AERONET daily data, which suggests that the AOD trends derived from satellite measurements of 1–2 overpasses may be representative of those from daily measurements.

Key words: MODIS, AERONET, Aerosol Optical Depth, Mann–Kendall trend test

Citation: Fan, X. H., X. A. Xia, and H. B. Chen, 2018: Can MODIS detect trends in aerosol optical depth over land? *Adv. Atmos. Sci.*, **35**(2), 135–145, https://doi.org/10.1007/s00376-017-7017-2.

1. Introduction

Aerosols remain one of the largest uncertainties in estimates and interpretation of the changes in Earth's energy budget (Boucher et al., 2013). Aerosol optical depth (AOD), which is related to the column-integrated aerosol amount, is a basic optical parameter used to estimate the aerosol radiative forcing. There is compelling reason to study long-term trends in AOD to help us ascertain the effects of aerosols on climate change. The Aerosol Robotic Network (AERONET) is a network of automated ground-based sunphotometers, which has been providing globally distributed, quality-assured observations of AOD since the 1990s (Holben et al., 1998). Observations were made over more than 7 years at 77 stations that are distributed around the world, which make the analysis of long-term trends in AOD possible. Linear trends in AOD and Ångström exponent values using AERONET level 2.0 aerosol products were reported by Xia (2011) and Yoon et al. (2012). Uncertainties in trends due to cloud disturbances were estimated using the weighted trends, depending on the monthly standard deviation (SD) and number of observations. Decreasing trends in AOD were observed in Western Europe, with the maximum trend of -0.12 (10 yr)$^{-1}$ at Belsk and North America, and with trends ranging from -0.04 (10 yr)$^{-1}$ at Egbert to -0.07 (10 yr)$^{-1}$ at MD_Science_Center (Xia, 2011). Li et al. (2014) presented trends in 440 nm AOD from 90 AERONET stations using two statistical methods—the Mann–Kendall (MK) test with Sen's slope estimator and linear least-squares fitting. Negative trends in AOD were also found at most sites in North America and Europe. In addition, there were downward trends of -0.08, -0.06 and -0.03 (10 yr)$^{-1}$ at CUIABA-MIRANDA in South America and at Osaka and Shirahma in Japan. Significant increasing trends were found at Kanpur [0.08 (10 yr)$^{-1}$] in India and at Solar_Village [0.13 (10 yr)$^{-1}$] on the Arabian Peninsula. The authors noted that the trends derived from AERONET AOD measurements are more robust compared with those from AERONET inversion products.

AOD from satellite measurements can provide global AOD trends. A number of studies have assessed tendencies in AOD from several satellite products, such as those from the

* Corresponding author: Xuehua FAN
Email: fxh@mail.iap.ac.cn

Advanced Very High Resolution Radiometer (Mishchenko et al., 2007; Zhao et al., 2008), the Sea-viewing Wide Field-of-view Sensor (SeaWiFS; Yoon et al., 2011; Hsu et al., 2012), the Multi-angle Imaging SpectroRadiometer (MISR; Kahn et al., 2007), the Moderate Resolution Imaging Spectroradiometer (MODIS; Yu et al., 2009; Zhang and Reid, 2010; Zhang et al., 2017), and the Along Track Scanning Radiometer (Thomas et al., 2010). The AOD retrieval algorithms, underlying assumptions and uncertainties involved in creating the products differ between the satellite sensors (Petrenko et al., 2012). These AOD products have substantial discrepancies (Kokhanovsky et al., 2007; Mishchenko et al., 2007; Thomas et al., 2010). The discrepancies remain so large that they can hardly be utilized to obtain a consistent and unified AOD trend (Li et al., 2009). Especially on regional scales, the differences can be much larger and more complex. Note that most of the studies mentioned above focused on the AOD trends from satellites over the ocean. Few studies have been carried out on AOD trends using satellite aerosol products over land (Yoon et al., 2011; Hsu et al., 2012), where the aerosol and surface characteristics are more complicated than those over the ocean. Yoon et al. (2011) and Hsu et al. (2012) evaluated the linear trends of SeaWiFS AOD using AERONET measurements over a limited number of land and coastal sites. Significant positive trends derived from SeaWiFS AOD were found over the Arabian Peninsula, India, southern China and eastern China, with linear slopes of 0.0092 ± 0.0013, 0.0063 ± 0.0020, 0.0049 ± 0.0018 and 0.0032 ± 0.0018 yr^{-1}, respectively. However, Li et al. (2014) reported declines of -0.10 and -0.18 (10 yr)$^{-1}$ in AERONET AOD at Beijing (2002–13) and Xianghe (2005–12) on the North China Plain. Negative AOD trends over the east coastal region of China since 2008 were also revealed by MODIS and MISR satellite measurements (Zhang et al., 2017).

Several recent studies have analyzed aerosol variations and trends using different models and data from multiple platforms. Chin et al. (2014) investigated aerosol tendencies and variations over a period of 30 years (1980–2009) using the Goddard Chemistry Aerosol Radiation and Transport model and multiple satellite sensors and ground-based networks. They found that the model-calculated global annually averaged AOD values showed little trend—a result that highlights the necessity of studying regional-scale AOD trends. Pozzer et al. (2015) compared the AOD trends from MODIS, SeaWiFS and MISR satellite measurements with simulated values from the ECHAM/Modular Earth Submodel System Atmospheric Chemistry (EMAC) general circulation model covering the decade (2001–10) on a global scale. The simulation results showed that the model could qualitatively reproduce the MODIS AOD trends over North America, Eastern Europe, North Africa and the Middle East, while some discrepancies were found for other regions. The application of a newly developed satellite AOD dataset, such as the MODIS collection 6, will be helpful to improve the reliability of these datasets and reduce artificial trends (Lyapustin et al., 2014; Pozzer et al., 2015).

The MODIS sensor onboard NASA's Aqua satellite has been collecting valuable data about the Earth system for more than 14 years, which has made it possible to detect the long-term variation in aerosol loading across the globe. However, the long-term AOD trends derived from MODIS need careful validation and assessment, especially over land. It is necessary to compare the AOD trends from the MODIS sensor with those from ground-based observations, which was the primary objective of the present study. Furthermore, most satellite aerosol products are derived from polar-orbiting satellites that pass overhead at a fixed time of day; for example, Terra passes overhead at 1010–1130 LST and Aqua passes overhead at 1230–1400 LST. Therefore, only 1–2 overpasses with aerosol retrievals collected at a fixed time of the day are available from these polar-orbiting satellites. When we use these satellite aerosol products to study long-term trends, one question that arises is whether the long-term AOD trend derived from satellite measurements of 1–2 overpasses can be representative of that determined from daily measurements. This was the second objective of the present work, which is somewhat similar to the analysis performed by Kaufman et al. (2000), who investigated whether daily aerosol abundances and properties could be represented by the aerosol products from the Terra and Aqua polar orbiting satellites. They showed that the annual average AOD could be calculated from Terra and Aqua aerosol products within a 2% error level, and this conclusion was independent of the particle size or range of the AOD.

2. Data and method

2.1. *Multi-sensor Aerosol Products Sampling System AOD*

The Multi-sensor Aerosol Products Sampling System (MAPSS) is a framework that provides statistics on spatial and temporal subsets of level 2.0 aerosol scientific datasets from spaceborne sensors as MODIS and MISR. The data system is described in detail in Petrenko et al. (2012). The AERONET sites were identified as focal points for spatial statistics. The process of generating the statistics for each spatial spaceborne aerosol product involved extracting values of the pixels that fell within a diameter of approximately 50 km centered on the chosen AERONET site. Statistics for ground-based temporal observations collected at a particular station were derived from measurements taken within ±30 min of each satellite overpass of this location. The MODIS dataset obtained from MAPSS used in this paper is a merged dataset comprising the dark target (DT) and deep blue (DB) AOD products filtered by quality assurance (QA) processes. Unless otherwise specified, all the analyses in this paper are based on AOD at 550 nm. The highest quality (QA = 3) AODs retrieved by the DB algorithm have been shown to have an absolute uncertainty of approximately $0.03 + 0.20\tau_M$ for a typical Atmosphere Mass Factor of 2.8 (Sayer et al., 2013), where τ_M is MODIS retrieved AOD. The uncertainty of MODIS DT AOD has been estimated to be $0.05 + 0.15\tau_A$ over land (Levy et al., 2010, 2013), where τ_A is collocated AERONET

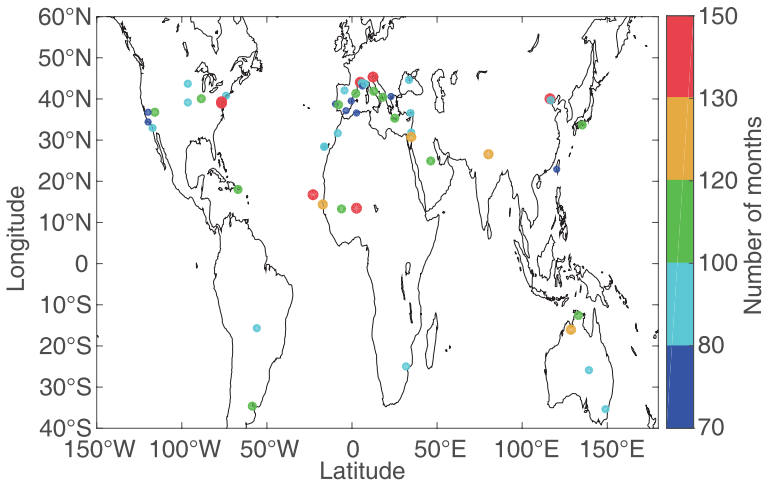

Fig. 1. Spatial distribution of stations with at least 70 months of monthly median AOD during 2002–15. The data length is represented by the colors.

AOD. Data at 53 AERONET stations were chosen for this analysis because their measurements are available for a relatively longer period compared with other stations. Figure 1 shows the spatial distribution of these stations, with their data lengths represented by the colors.

2.2. *Data analysis*

We used quality-assured and cloud-screened level 2.0 AERONET AOD data, with a low uncertainty of 0.01–0.02 (Holben et al., 1998). Three daily series were calculated from instantaneous AOD products as follows: AERONET daily mean AOD was calculated from all instantaneous AOD measurements each day; AERONET morning and afternoon mean AOD was calculated from instantaneous AOD measurements within ±30 min of the Terra and Aqua overpass times; and monthly median AOD was calculated from the daily mean AERONET AOD if there were more than five daily measurements each month [AOD reference value (AOD_{RE})], which was taken as a benchmark for comparison with other estimates. The monthly median AOD in the morning (AOD_{AM}) and in the afternoon (AOD_{PM}) were also calculated if at least five daily measurements were available each month. The monthly median was used in the trend test instead of the monthly mean because AOD does not follow a normal distribution. The AOD trends derived from AOD_{RE}, AOD_{AM} and AOD_{PM} were compared to determine whether the trends derived from AERONET AOD measured at the Terra and Aqua overpass times were representative of those derived from daily mean AERONET AOD. The monthly medians of AOD_{MOD} were calculated from all collocated AOD from MODIS/Aqua provided by the MAPSS system if there were more than five daily measurements each month. The AOD trends from AOD_{MOD} were compared with those of AOD_{RE} to determine whether AERONET AOD trends could be reproduced by MODIS. The trends from AERONET and MODIS/Aqua AOD at each site were calculated based on the measurements during the same measurement period. Although the comparison of the AOD_{RE} and AOD_{MOD} trends mentioned above was based on measurements during the same study period, AOD measurements were not necessarily available simultaneously from AERONET and MODIS each day. Therefore, the monthly median AOD from AERONET and MODIS were probably calculated from different daily measurements. In other words, it was possible that daily AOD was available from AERONET, but MODIS/Aqua had no AOD product, or vice versa. This situation arose because of insufficient temporal coverage by MODIS or insufficient spatial coverage by AERONET. Since the difference in temporal sampling was not considered in calculating the monthly median AOD values, the trends in the MODIS and AERONET data may not have been consistent. The AOD measurements from AERONET and MODIS/Aqua were matched day-by-day, and the monthly medians were then recalculated for all the sites to assess the potential effects of sampling issues on the comparison of AOD trends.

2.3. *Trend detection*

The MK test was used to detect monotonic trends. The MK test is a rank-based non-parametric test for assessing the significance of a trend, which requires that the data be independent. The null hypothesis (H_0) is that a sample of data, $\{X_1, X_2 \ldots, X_n\}$, is independent and identically distributed. The alternative hypothesis (H_1) is that a monotonic trend exists in $\boldsymbol{X}$. The slope b of the trend is computed using the method proposed by Sen (1968) as follows:

$$b = \text{Median}\left(\frac{X_i - X_j}{i - j}\right), \quad \forall i > j\,, \tag{1}$$

where b is the slope of the trend, X_i and X_j are the ith and the jth observations respectively. The slope is robust for estimating the magnitude of a trend (Yue and Wang, 2002) and much less sensitive to outliers compared with linear regression coefficient (Li et al., 2014).

The non-parametric test is more suitable for non-normally distributed, censored, and missing data (Yue and Wang, 2002), such as the AERONET AOD data (Li et al., 2014).

However, the AOD time series, which have distinct seasonal variability, frequently display statistically significant serial correlation. The existence of positive serial correlation in a time series increases the probability of the MK test detecting a significant trend (Hirsch and Slack, 1984; Yue and Wang, 2002). Therefore, a pre-whitening scheme proposed by Yue et al. (2002) was used to eliminate the influence of serial correlation on the MK trend detections. First, the slope (b) of the trend in an AOD time series was estimated using Eq. (1). If b was almost equal to zero, then it was not necessary to continue performing the trend analysis. If it differed from zero, the AOD time series were detrended using

$$X'_t = X_t - T_t = X_t - bt \,, \tag{2}$$

where X'_t is the 'trend-removed' residual series, X_t denotes the raw AOD time series, and T_t is the identified trend with the slope b of the trend at time t. Second, the lag-1 autocorrelation component was removed from the detrended time series (X'_t) using

$$Y'_t = X'_t - r_1 X'_{t-1} \,, \tag{3}$$

where r_1 is the lag-1 autocorrelation coefficient, X'_{t-1} is the detrended series at time $t-1$. Third, the identified trend was added back to the residual Y'_t according to the following equation:

$$Y_t = Y'_t + T_t \,. \tag{4}$$

It was evident that the blended time series (Y_t) preserved the true trend and was no longer influenced by the effects of autocorrelation. The MK test and Sen's slope estimator were applied to the blended series to estimate the trend in AOD time series. Hirsch and Slack (1984) developed a seasonal MK test and estimated the annual trend as the median of the seasonal trends—an approach that is resistant to data seasonality and serial dependence. Thus, the pre-whitening scheme described by Yue et al. (2002) was adopted first. Then, the seasonal MK test of Hirsch and Slack (1984) and Sen's slope estimator were applied to the pre-whitened time series of AOD.

3. Results and discussion

Table 1 shows that relatively low monthly mean AOD (< 0.15) was found in Australia, Europe, North America and South America, except at CUIABA-MIRANDA, where the aerosols were influenced by biomass burning in the Amazon region. The sites located in the semi-arid Sahel region (such as Banizoumbou, Dakar, and IER_Cinzana), and in East Asia (Beijing and Chen-Kung_Univ), as well as northern India (Kanpur), showed higher monthly mean AOD (> 0.35).

Table 2 shows that the majority of sites exhibited negative trends of $\mathrm{AOD_{RE}}$, including all stations in Europe, North America, South America and most sites in Africa (eight of nine) and Asia (seven of nine), although the trends were not statistically significant at some sites. A significant increasing trend in $\mathrm{AOD_{RE}}$ [0.12 $(10\ \mathrm{yr})^{-1}$] was found only at Solar_Village in Saudi Arabia. The strong positive trend there has also been noted in AOD measurements collected by SeaWiFS (Hsu et al., 2012), MISR (de Meij et al., 2012a) and MODIS/Aqua (this study), as well as EMAC model simulations (de Meij et al., 2012b; Pozzer et al., 2015). $\mathrm{AOD_{RE}}$ at Skukuza in South Africa, Kanpur in India, and Birdsville in Australia showed trends that were increasing but were not statistically significant.

Comparisons of the trends between $\mathrm{AOD_{RE}}$ and $\mathrm{AOD_{AM}}$, between $\mathrm{AOD_{RE}}$ and $\mathrm{AOD_{PM}}$, and between $\mathrm{AOD_{RE}}$ and $\mathrm{AOD_{MOD}}$ are illustrated in Figs. 2–4, respectively. The tendencies in $\mathrm{AOD_{RE}}$ were reproduced by $\mathrm{AOD_{AM}}$ and $\mathrm{AOD_{PM}}$ at nearly all stations. The trend magnitudes of $\mathrm{AOD_{AM}}$ and $\mathrm{AOD_{PM}}$ were also close to those from $\mathrm{AOD_{RE}}$ at most stations. The results suggest that AOD measured at Terra or Aqua overpass times could represent the trends derived from daily measurements.

The trends in $\mathrm{AOD_{RE}}$ and $\mathrm{AOD_{MOD}}$ were consistent over 44 of the sites. All sites in Europe and North America showed the same tendencies. Opposite MK trends between $\mathrm{AOD_{RE}}$ and $\mathrm{AOD_{MOD}}$ were found at one of nine sites in Africa (Banizoumbou), four of nine sites in Asia (Beijing, Xianghe, Nes_Ziona and SEDE_BOKER), three of four sites in Oceania (Birdsville, Canberra and Jabiru), and three of four sites in South America (CEILAP-BA, La_Parguera, and Trelew).

The tendencies of the strictly matched monthly medians of $\mathrm{AOD_{RE}}$ and $\mathrm{AOD_{MOD}}$ (i.e., monthly medians calculated from simultaneous measurements from both products) remained unchanged except at Beijing in China, which suggests that the temporal differences in sampling between $\mathrm{AOD_{RE}}$ and $\mathrm{AOD_{MOD}}$ has little effect on the detection of AOD trends in most cases. If the temporal sampling difference was not accounted for, the $\mathrm{AOD_{RE}}$ at Beijing showed a significant decreasing trend [$-0.08\ (10\ \mathrm{yr})^{-1}$] but the $\mathrm{AOD_{MOD}}$ exhibited a weak increasing trend [$0.01\ (10\ \mathrm{yr})^{-1}$]. The trend in $\mathrm{AOD_{MOD}}$ changed to $-0.03\ (10\ \mathrm{yr})^{-1}$ if the daily measurements from AERONET and MODIS/Aqua were strictly matched. Additionally, the seasonal MK tests of MODIS and AERONET AOD exhibited the same trend signs at Xianghe as those reported by Zhang et al. (2017). Increasing trends of $0.001\ \mathrm{yr}^{-1}$ (MODIS) and $0.004\ \mathrm{yr}^{-1}$ (AERONET) were found from 2002 to 2007, but there were downward trends of $-0.006\ \mathrm{yr}^{-1}$ (MODIS) and $-0.004\ \mathrm{yr}^{-1}$ (AERONET) from 2008 to 2015. However, consistent declines in AERONET AOD and MODIS/Aqua AOD were found at Beijing during the two periods (2002–07 and 2008–15).

AOD over Australia is typically low, with occasional high AOD events mostly resulting from locally derived or transported smoke from wildfires and mineral dust (Qin and Mitchell, 2009). Another interesting feature seen in this region is that the surface reflectance is relatively high, because of the abundance of bare soil and desert. Both factors indicate that it is very hard to retrieve AOD with high quality. Validation has shown that the correlation between AERONET and MODIS AOD is lower over Australia than in other regions (Sayer et al., 2013). Figure 5a shows the time series of the monthly medians of $\mathrm{AOD_{RE}}$ and $\mathrm{AOD_{MOD}}$ (shown as a dependent variable on the left-hand y-axis) and the AOD anomaly (shown as a dependent variable on the right-hand y-axis) defined as the difference between the

Table 1. Site locations, study periods and 550-nm monthly mean AOD ± SD from the four data records at the 53 selected stations. AOD_{RE} is monthly mean AOD calculated from the daily AERONET AOD if there were more than five daily measurements each month. AOD_{AM} and AOD_{PM} is monthly mean AOD calculated from AERONET instantaneous AOD measurements within ±30 min of the Terra and Aqua overpass times. AOD_{MOD} were calculated from all collocated AOD from MODIS/Aqua provided by the MAPSS system if there were more than five daily measurements each month.

Site	Latitude, longitude	Study period	Averaged AOD			
			AOD_{RE}	AOD_{AM}	AOD_{PM}	AOD_{MOD}
Africa						
Banizoumbou	13.5°N, 2.7°E	2002.7–2015.4	0.44 ± 0.23	0.44 ± 0.23	0.44 ± 0.23	0.42 ± 0.22
Blida	36.5°N, 2.9°E	2003.11–2010.10	0.17 ± 0.09	0.18 ± 0.09	0.20 ± 0.09	0.14 ± 0.07
Capo_Verde	16.7°N, 22.9°W	2002.7–2015.4	0.25 ± 0.13	0.26 ± 0.14	0.25 ± 0.13	0.30 ± 0.13
Dakar	14.4°N, 17.0°W	2003.6–2015.4	0.39 ± 0.17	0.38 ± 0.16	0.39 ± 0.18	0.32 ± 0.16
IER_Cinzana	13.3°N, 5.9°W	2004.6–2015.4	0.40 ± 0.18	0.39 ± 0.18	0.40 ± 0.18	0.34 ± 0.18
La_Laguna	28.5°N, 16.3°W	2006.7–2014.8	0.15 ± 0.10	0.15 ± 0.10	0.15 ± 0.10	0.18 ± 0.09
Saada	31.6°N, 8.2°W	2004.7–2015.4	0.17 ± 0.10	0.17 ± 0.09	0.16 ± 0.09	0.12 ± 0.04
Santa_Cruz_Tenerife	28.5°N, 16.3°W	2005.7–2013.12	0.14 ± 0.08	0.14 ± 0.08	0.14 ± 0.08	0.18 ± 0.08
Skukuza	25.0°S, 31.6°E	2002.7–2011.7	0.16 ± 0.07	0.17 ± 0.08	0.16 ± 0.07	0.11 ± 0.07
Asia						
Beijing	40.0°N, 116.4°E	2002.7–2015.4	0.35 ± 0.22	0.32 ± 0.24	0.37 ± 0.25	0.46 ± 0.25
Chen-Kung_Univ	23.0°N, 120.2°E	2002.7–2015.4	0.49 ± 0.20	0.49 ± 0.21	0.46 ± 0.18	0.59 ± 0.18
IMS-METU-ERDEMLI	36.6°N, 34.3°E	2003.2–2014.12	0.19 ± 0.08	0.19 ± 0.08	0.18 ± 0.07	0.18 ± 0.07
Kanpur	26.5°N, 80.2°E	2002.7–2014.6	0.58 ± 0.18	0.58 ± 0.19	0.58 ± 0.19	0.58 ± 0.19
Nes_Ziona	31.9°N, 34.8°E	2002.7–2014.10	0.17 ± 0.04	0.19 ± 0.05	0.17 ± 0.04	0.21 ± 0.05
SEDE_BOKER	30.9°N, 34.8°E	2002.7–2015.4	0.13 ± 0.04	0.13 ± 0.04	0.13 ± 0.05	0.27 ± 0.07
Shirahama	33.7°N, 135.4°E	2002.7–2015.4	0.19 ± 0.08	0.17 ± 0.09	0.19 ± 0.08	0.23 ± 0.08
Solar_Village	24.9°N, 46.4°E	2002.7–2013.4	0.31 ± 0.14	0.29 ± 0.14	0.31 ± 0.14	0.27 ± 0.12
Xianghe	39.8°N, 117.0°E	2004.9–2015.4	0.34 ± 0.21	0.33 ± 0.23	0.34 ± 0.20	0.38 ± 0.29
Australia						
Birdsville	25.9°S, 139.4°E	2005.8–2013.9	0.03 ± 0.02	0.03 ± 0.02	0.03 ± 0.02	0.05 ± 0.03
Canberra	35.3°S, 149.1°E	2003.11–2015.4	0.05 ± 0.02	0.05 ± 0.02	0.05 ± 0.02	0.04 ± 0.02
Jabiru	12.7°S, 132. 9°E	2002.7–2014.12	0.13 ± 0.08	0.13 ± 0.082	0.13 ± 0.08	0.08 ± 0.06
Lake_Argyle	16.1°S, 128.8°E	2002.7–2015.4	0.11 ± 0.08	0.10 ± 0.08	0.11 ± 0.08	0.07 ± 0.05
Europe						
Avignon	43.9°N, 4.9°E	2002.7–2012.10	0.14 ± 0.06	0.14 ± 0.06	0.13 ± 0.05	0.15 ± 0.06
Barcelona	41.4°N, 2.1°E	2004.12–2015.1	0.13 ± 0.06	0.12 ± 0.06	0.13 ± 0.06	0.15 ± 0.07
Burjassot	39.5°N, 0.4°W	2007.5–2015.4	0.12 ± 0.05	0.12 ± 0.06	0.11 ± 0.04	0.10 ± 0.05
Cabo_da_Roca	38.8°N, 9.5°W	2003.11–2015.4	0.10 ± 0.05	0.10 ± 0.06	0.11 ± 0.05	0.14 ± 0.08
Carpentras	44.1°N, 5.1°E	2003.2–2015.4	0.11 ± 0.05	0.11 ± 0.05	0.11 ± 0.05	0.14 ± 0.06
Evora	38.6°N, 7.9°W	2003.7–2014.10	0.12 ± 0.06	0.12 ± 0.07	0.13 ± 0.07	0.09 ± 0.06
FORTH_CRETE	35.3°N, 25.3°E	2003.3–2013.9	0.14 ± 0.04	0.14 ± 0.04	0.14 ± 0.04	0.18 ± 0.05
Granada	37.2°N, 3.6°W	2005.1–2014.12	0.12 ± 0.04	0.12 ± 0.04	0.12 ± 0.05	0.13 ± 0.05
Lecce_University	40.3°N, 18.1°E	2003.3–2013.11	0.18 ± 0.06	0.19 ± 0.06	0.18 ± 0.06	0.12 ± 0.05
OHP_OBSERVATOIRE	43.9°N, 5.7°E	2005.6–2014.10	0.08 ± 0.04	0.08 ± 0.04	0.09 ± 0.04	0.09 ± 0.05
Palencia	42.0°N, 4.5°W	2003.4–2015.4	0.08 ± 0.03	0.08 ± 0.03	0.07 ± 0.03	0.09 ± 0.05
Rome_Tor_Vergata	41.8°N, 12.7°E	2002.9–2015.4	0.14 ± 0.05	0.14 ± 0.05	0.16 ± 0.06	0.17 ± 0.06
Sevastopol	44.6°N, 33.5°E	2006.6–2013.8	0.15 ± 0.04	0.15 ± 0.05	0.15 ± 0.05	0.14 ± 0.04
Thessaloniki	40.6°N, 23.0°E	2005.10–2015.4	0.18 ± 0.07	0.19 ± 0.08	0.17 ± 0.07	0.20 ± 0.10
Toulon	43.1°N, 6.0°E	2004.11–2015.4	0.10 ± 0.05	0.10 ± 0.05	0.11 ± 0.05	0.12 ± 0.06
Venise	45.3°N, 12.5°E	2002.7–2015.4	0.21 ± 0.06	0.22 ± 0.07	0.20 ± 0.07	0.25 ± 0.08
Villefranche	43.7°N, 7.3°E	2004.1–2014.5	0.13 ± 0.06	0.12 ± 0.06	0.13 ± 0.06	0.15 ± 0.07
North America						
BONDVILLE	40.1°N, 88.4°W	2002.7–2014.9	0.11 ± 0.06	0.11 ± 0.08	0.11 ± 0.07	0.14 ± 0.08
CCNY	40.8°N, 74.0°W	2002.7–2015.4	0.08 ± 0.04	0.08 ± 0.04	0.09 ± 0.06	0.21 ± 0.13
Frenchman_Flat	36.8°N, 15.9°W	2006.11–2014.7	0.05 ± 0.02	0.05 ± 0.02	0.05 ± 0.02	0.06 ± 0.03
Fresno	36.8°N, 19.8°W	2002.7–2011.12	0.13 ± 0.05	0.14 ± 0.06	0.12 ± 0.05	0.13 ± 0.05
GSFC	39.0°N, 76.8°W	2002.7–2014.6	0.12 ± 0.10	0.12 ± 0.09	0.12 ± 0.11	0.19 ± 0.15
KONZA_EDC	39.1°N, 96.6°W	2002.7–2014.9	0.11 ± 0.08	0.10 ± 0.08	0.11 ± 0.08	0.07 ± 0.05
La_Jolla	32.9°N, 17.3°W	2003.2–2013.10	0.08 ± 0.03	0.09 ± 0.03	0.08 ± 0.03	0.09 ± 0.05
MD_Science_Center	39.3°N, 76.6°W	2002.7–2014.10	0.10 ± 0.68	0.10 ± 0.07	0.11 ± 0.08	0.15 ± 0.09
Sioux_Falls	43.7°N, 96.6°W	2002.7–2015.4	0.10 ± 0.05	0.10 ± 0.05	0.10 ± 0.05	0.13 ± 0.07
UCSB	34.4°N, 19.8°W	2003.2–2014.12	0.08 ± 0.05	0.08 ± 0.05	0.08 ± 0.04	0.06 ± 0.04
South America						
CEILAP-BA	34.6°S, 58.5°W	2002.8–2013.7	0.07 ± 0.02	0.07 ± 0.02	0.08 ± 0.02	0.14 ± 0.05
CUIABA-MIRANDA	15.7°S, 56.0°W	2003.4–2014.10	0.23 ± 0.23	0.24 ± 0.24	0.23 ± 0.23	0.19 ± 0.28
La_Parguera	18.0°N, 67.1°W	2002.7–2015.4	0.11 ± 0.07	0.11 ± 0.07	0.12 ± 0.07	0.17 ± 0.08
Trelew	43.2°S, 65.3°W	2005.11–2014.8	0.03 ± 0.02	0.03 ± 0.01	0.03 ± 0.02	0.05 ± 0.03

Table 2. Site locations, study periods and decadal trends in 550-nm AOD from the four data records at the 53 selected stations. Bold font indicates trends that are statistically significant at the 95% confidence level.

Site	Latitude, longitude	Study period	MK trend of AOD (10 yr^{-1})			
			AOD_{RE}	AOD_{AM}	AOD_{PM}	AOD_{MOD}
Africa						
Banizoumbou	13.5°N, 2.7°E	2002.7–2015.4	−0.01	−0.01	−0.00	0.02
Blida	36.5°N, 2.9°E	2003.11–2010.10	−0.07	−0.06	−0.05	−0.03
Capo_Verde	16.7°N, 22.9°W	2002.7–2015.4	**−0.05**	−0.03	−0.02	−0.06
Dakar	14.4°N, 17.0°W	2003.6–2015.4	**−0.08**	**−0.09**	−0.09	−0.04
IER_Cinzana	13.3°N, 5.9°W	2004.6–2015.4	**−0.05**	−0.06	**−0.06**	−0.04
La_Laguna	28.5°N, 16.3°W	2006.7–2014.8	−0.01	−0.01	−0.01	−0.01
Saada	31.6°N, 8.2°W	2004.7–2015.4	**−0.04**	**−0.04**	**−0.04**	**−0.01**
Santa_Cruz_Tenerife	28.5°N, 16.3°W	2005.7–2013.12	−0.07	−0.06	−0.07	−0.04
Skukuza	25.0°S, 31.6°E	2002.7–2011.7	0.02	0.02	0.01	**0.05**
Asia						
Beijing	40.0°N, 116.4°E	2002.7–2015.4	**−0.08**	−0.07	**−0.10**	0.01
Chen-Kung_Univ	23.0°N, 120.2°E	2002.7–2015.4	−0.07	**−0.08**	−0.06	**−0.10**
IMS-METU-ERDEMLI	36.6°N, 34.3°E	2003.2–2014.12	−0.02	−0.01	−0.01	−0.00
Kanpur	26.5°N, 80.2°E	2002.7–2014.6	0.03	**0.07**	0.03	0.05
Nes_Ziona	31.9°N, 34.8°E	2002.7–2014.10	−0.02	−0.02	**−0.03**	0.01
SEDE_BOKER	30.9°N, 34.8°E	2002.7–2015.4	−0.01	−0.01	**−0.01**	**0.04**
Shirahama	33.7°N, 135.4°E	2002.7–2015.4	**−0.05**	**−0.03**	−0.01	−0.01
Solar_Village	24.9°N, 46.4°E	2002.7–2013.4	**0.13**	**0.14**	**0.12**	**0.09**
Xianghe	39.8°N, 117.0°E	2004.9–2015.4	−0.01	−0.01	0.00	0.04
Australia						
Birdsville	25.9°S, 139.4°E	2005.8–2013.9	0.01	0.01	0.01	**−0.07**
Canberra	35.3°S, 149.1°E	2003.11–2015.4	−0.00	−0.00	−0.00	**0.01**
Jabiru	12.7°S, 132. 9°E	2002.7–2014.12	−0.02	−0.01	−0.01	0.01
Lake_Argyle	16.1°S, 128.8°E	2002.7–2015.4	0.00	0.00	0.00	0.00
Europe						
Avignon	43.9°N, 4.9°E	2002.7–2012.10	**−0.04**	**−0.04**	**−0.05**	−0.02
Barcelona	41.4°N, 2.1°E	2004.12–2015.1	**−0.06**	**−0.05**	**−0.07**	**−0.05**
Burjassot	39.5°N, 0.4°W	2007.5–2015.4	−0.01	−0.00	−0.00	−0.02
Cabo_da_Roca	38.8°N, 9.5°W	2003.11–2015.4	**−0.03**	−0.02	**−0.02**	**−0.03**
Carpentras	44.1°N, 5.1°E	2003.2–2015.4	**−0.05**	**−0.04**	**−0.05**	**−0.04**
Evora	38.6°N, 7.9°W	2003.7–2014.10	**−0.03**	**−0.03**	**−0.03**	−0.01
FORTH_CRETE	35.3°N, 25.3°E	2003.3–2013.9	**−0.03**	**−0.03**	**−0.03**	−0.01
Granada	37.2°N, 3.6°W	2005.1–2014.12	−0.02	−0.01	−0.03	**−0.02**
Lecce_University	40.3°N, 18.1°E	2003.3–2013.11	**−0.03**	−0.03	−0.01	−0.01
OHP_OBSERVATOIRE	43.9°N, 5.7°E	2005.6–2014.10	−0.01	−0.00	−0.01	−0.00
Palencia	42.0°N, 4.5°W	2003.4–2015.4	**−0.03**	−0.06	**−0.07**	−0.03
Rome_Tor_Vergata	41.8°N, 12.7°E	2002.9–2015.4	**−0.03**	**−0.03**	−0.05	**−0.05**
Sevastopol	44.6°N, 33.5°E	2006.6–2013.8	−0.03	−0.03	−0.02	−0.05
Thessaloniki	40.6°N, 23.0°E	2005.10–2015.4	−0.04	**−0.09**	−0.06	−0.03
Toulon	43.1°N, 6.0°E	2004.11–2015.4	**−0.03**	−0.03	−0.03	−0.02
Venise	45.3°N, 12.5°E	2002.7–2015.4	**−0.06**	**−0.07**	**−0.06**	**−0.06**
Villefranche	43.7°N, 7.3°E	2004.1–2014.5	**−0.03**	**−0.05**	**−0.04**	−0.02
North America						
BONDVILLE	40.1°N, 88.4°W	2002.7–2014.9	−0.01	−0.00	−0.01	−0.02
CCNY	40.8°N, 74.0°W	2002.7–2015.4	−0.02	−0.02	**−0.03**	**−0.03**
Frenchman_Flat	36.8°N, 15.9°W	2006.11–2014.7	**−0.02**	−0.00	−0.00	−0.00
Fresno	36.8°N, 19.8°W	2002.7–2011.12	−0.01	−0.03	−0.01	−0.01
GSFC	39.0°N, 76.8°W	2002.7–2014.6	**−0.01**	−0.00	−0.00	**−0.05**
KONZA_EDC	39.1°N, 96.6°W	2002.7–2014.9	−0.00	−0.00	−0.01	−0.01
La_Jolla	32.9°N, 17.3°W	2003.2–2013.10	**−0.02**	−0.01	−0.01	−0.02
MD_Science_Center	39.3°N, 76.6°W	2002.7–2014.10	**−0.03**	**−0.02**	**−0.01**	−0.03
Sioux_Falls	43.7°N, 96.6°W	2002.7–2015.4	−0.00	−0.00	−0.01	−0.01
UCSB	34.4°N, 19.8°W	2003.2–2014.12	−0.02	**−0.03**	**−0.04**	**−0.02**
South America						
CEILAP-BA	34.6°S, 58.5°W	2002.8–2013.7	**−0.01**	**−0.02**	−0.00	0.01
CUIABA-MIRANDA	15.7°S, 56.0°W	2003.4–2014.10	**−0.08**	**−0.08**	**−0.07**	**−0.06**
La_Parguera	18.0°N, 67.1°W	2002.7–2015.4	−0.01	−0.01	−0.00	0.01
Trelew	43.2°S, 65.3°W	2005.11–2014.8	**−0.01**	−0.00	−0.00	**0.03**

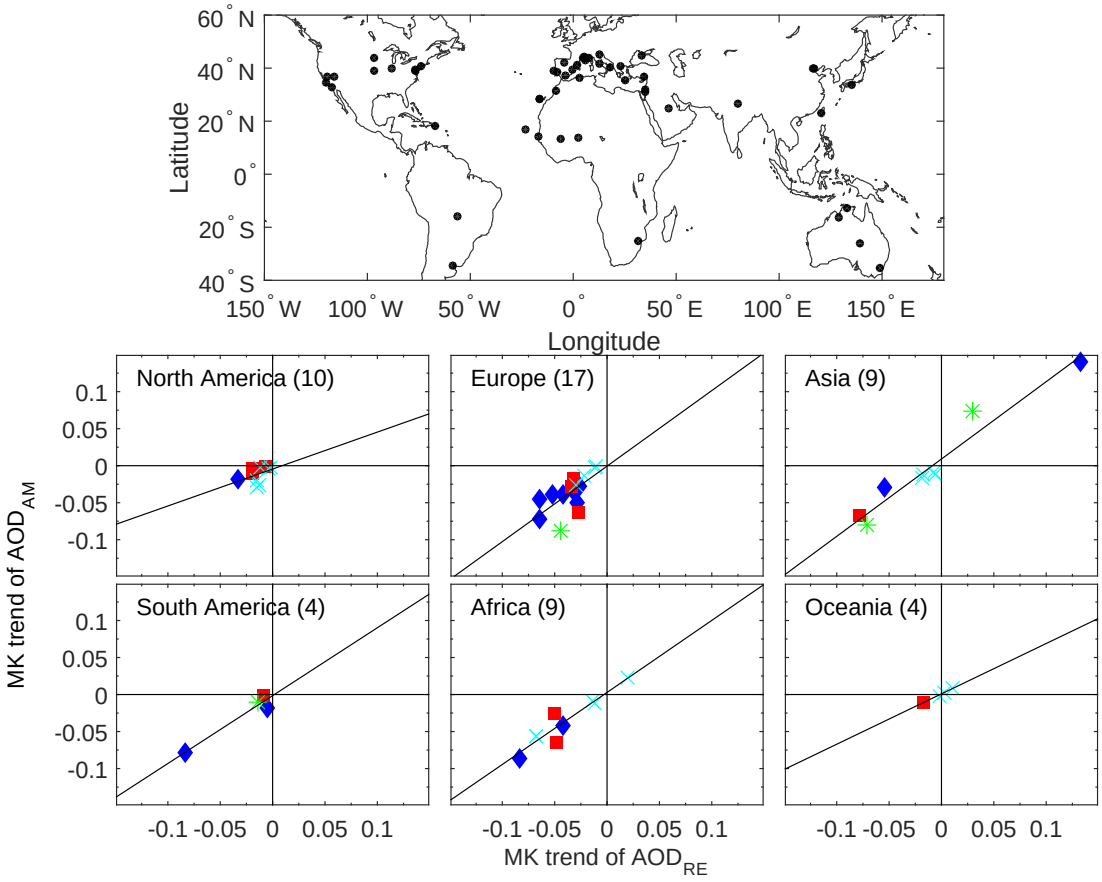

Fig. 2. Comparison of decadal trends between AOD_{RE} and AOD_{AM} in different regions. The trends estimated from AOD_{RE} and AOD_{AM} are shown on the *x*-axes and the *y*-axes, respectively, in the scatterplots. Blue solid diamonds indicate that the trends from both AOD_{RE} and AOD_{AM} were statistically significant. Red solid squares indicate that the AOD_{RE} trend was statistically significant but the AOD_{AM} trend was statistically non-significant. Green asterisks indicate that the AOD_{RE} trend was statistically non-significant but the AOD_{AM} trend was statistically significant. Cyan crosses indicate that the trends from AOD_{RE} and AOD_{AM} were statistically non-significant. The black dots in the map represented the locations of sites, and the numbers of sites in the different regions are given in parentheses in the scatter-plots.

AOD_{MOD} and the monthly averaged AOD_{RE}over all years at Birdsville, Australia. An interesting feature is that all the AOD anomalies were positive before September 2008, i.e., MODIS/Aqua overestimated AOD, but AOD was underestimated by MODIS afterwards. The shift in the AOD anomalies resulted in the artificially negative trend in AOD_{MOD} seen at Birdsville. This same scenario also occurred at Canberra. Trelew is in the middle of the Argentinean Patagonia, where the monthly median AOD is less than 0.10. A shift in AOD anomalies after March 2008 (Fig. 5b) resulted in an artificially positive tendency in AOD_{MOD}. The reason for these abrupt changes in MODIS performance compared with AERONET at these stations needs further study.

Banizoumbou, in the semi-arid Sahel region and influenced by dust emissions and/or biomass burning (Levy et al., 2010), showed high AOD. Studies have shown that, from the mid-1980s to the mid-2000s in the Sahara and Sahel regions, near-surface wind speed decreased, precipitation increased, and therefore dust emissions decreased (Chin et al., 2014). This finding of a reduction in AOD is also supported by in-situ aerosol measurements (Li et al., 2014) and model simulations (Chin et al., 2014). The AOD_{RE} and AOD_{MOD} at other stations in the Sahel showed a declining trend. Therefore, the increasing trend at Banizoumbou (although non-significant) seen in the MODIS data seems likely to be spurious.

The sites of SEDE_BOKER and Nes_Ziona are in Israel, where aerosols are influenced both by mineral dust transported from the Saharan and Arabian deserts and fine-mode pollution emitted by the petroleum industry in this region (Yoon et al., 2012). The AOD at these two sites showed a decreasing tendency based on AERONET measurements, which is consistent with the results reported by Yoon et al. (2012) and Li et al. (2014). Yoon et al. (2012) noted that the decreased AERONET AOD at SEDE_BOKER was due to a decrease in coarse-mode particles [approximately -0.29 $(10\ \mathrm{yr})^{-1}$ for coarse-mode AOD]. MODIS/Aqua AOD generally produced overestimates at SEDE_BOKER, where 98% of the monthly median anomalies were positive (Fig. 5c). The

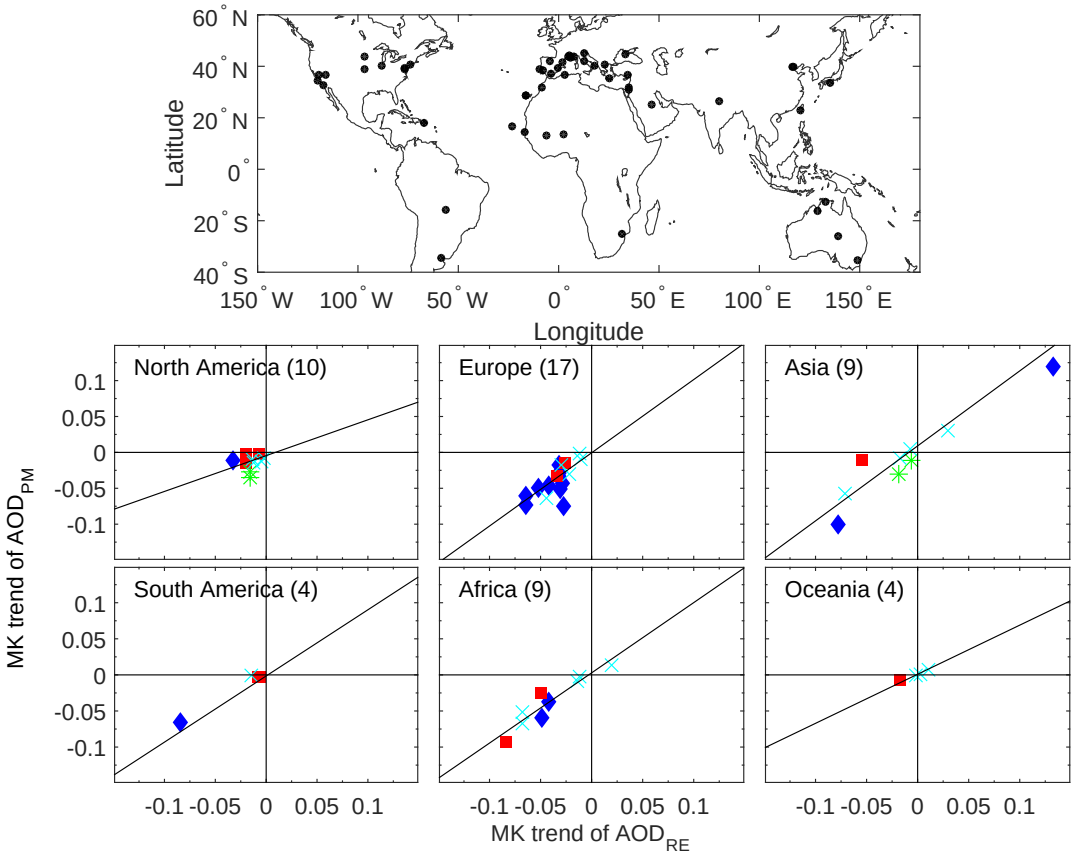

Fig. 3. As Fig. 2, except that the trend comparisons are between AOD_{RE} and AOD_{PM}.

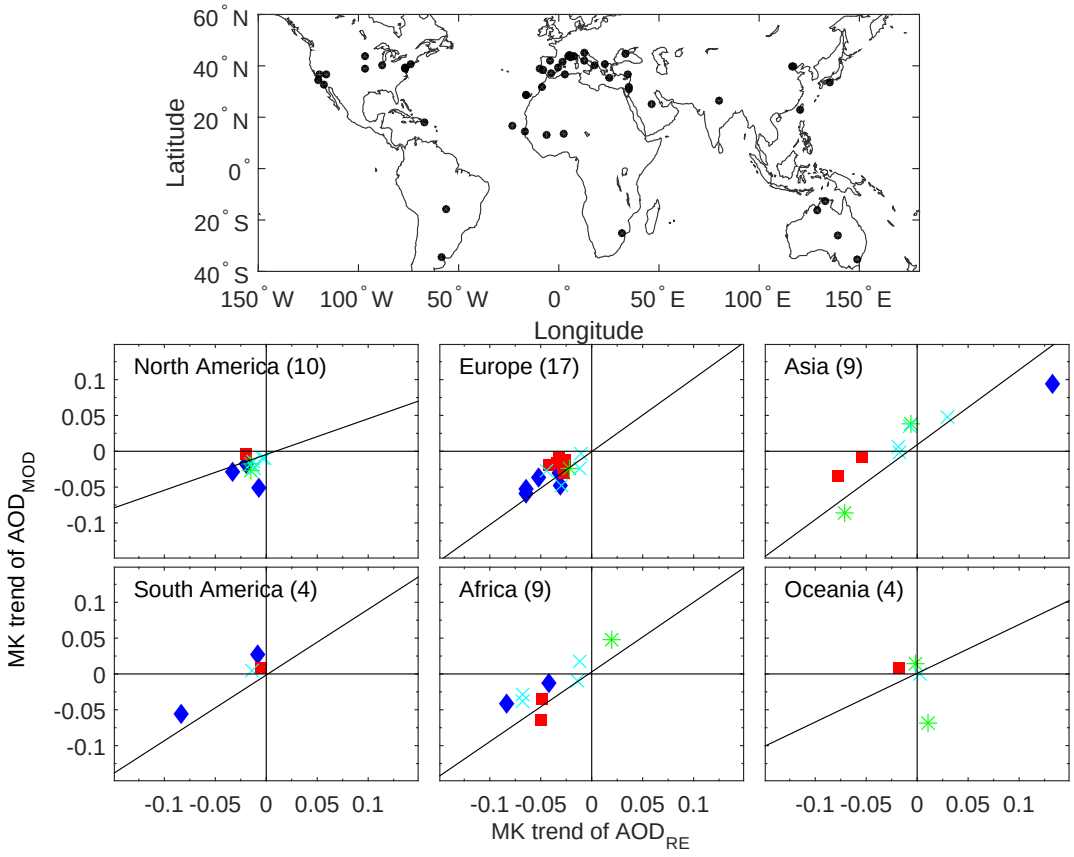

Fig. 4. As Fig. 2, except that the trend comparisons are between AOD_{RE} and AOD_{MOD}.

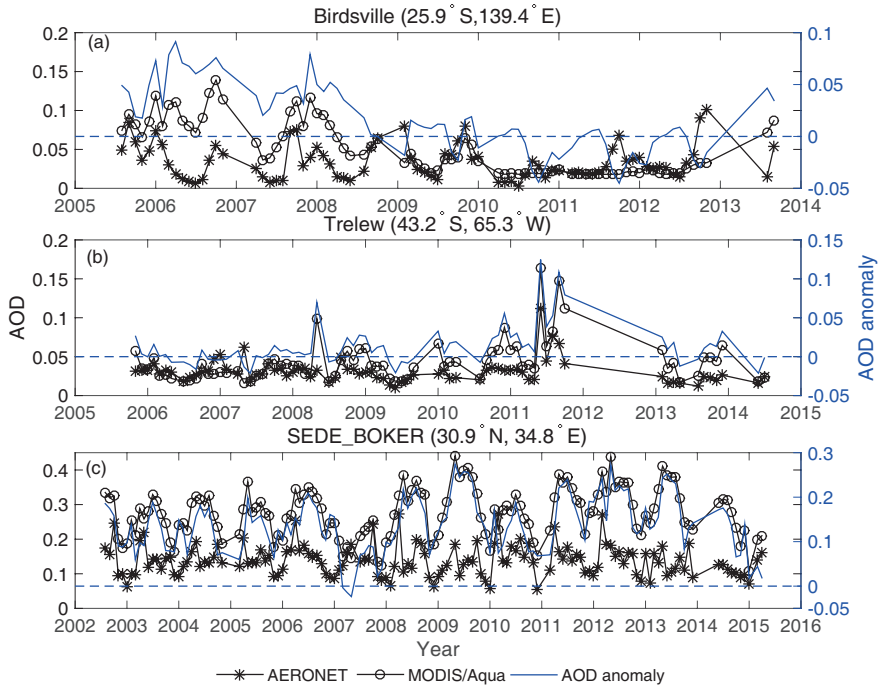

Fig. 5. Comparison of AERONET AOD (AOD_{RE}) and MODIS/Aqua AOD (AOD_{MOD}) at (a) Birdsville in Australia, (b) Trelew in Argentina, and (c) SEDE_BOKER in Israel. The AOD anomalies are shown as blue solid lines, which are matched to the right-hand ordinate axis, and the blue dashed lines indicate that the anomaly is 0.

retrieval uncertainty of MODIS AOD under conditions with heavy aerosol loading is mainly related to the aerosol mode assumptions. The MODIS retrieval algorithm assumes a constant single-scattering albedo value; however, the AERONET single-scattering albedo at SEDE_BOKER shows an increasing trend [0.004 $(10\ yr)^{-1}$] (Li et al., 2014). Therefore, the temporal change in single-scattering albedo may produce a spurious tendency in the AOD retrieved by MODIS (Mishchenko et al., 2007, 2012; Li et al., 2014).

In addition, we found a few high-altitude sites (> 1.2 km) in North America (BSRN_BAO_Boulder, Railroad_Valley, Sevilleta, TABLE_MOUNTAIN_CA) and Asia (Dalanzadgad) where AERONET AOD was not suitable for representing the regional AOD trend due to a lack of spatial representation. The retrieval accuracy of MODIS AOD at such sites is impacted by the weak aerosol signal due to the very low aerosol loading (Levy et al., 2010; Sayer et al., 2013). Thus, high-altitude sites (> 1.2 km) were excluded in the AOD trend analyses.

4. Conclusions

AOD trends derived from MODIS/Aqua and AERONET at 53 stations in land areas in various locations across the globe were compared and analyzed. The major findings can be summarized as follows:

AOD trends calculated from daily measurements can be accurately reproduced by AOD measurements collected at the overpass time of MODIS, which indicates that MODIS has the potential to capture AOD trends.

Consistent AOD tendencies calculated from the monthly medians of the AERONET and MODIS/Aqua AOD products were derived at 44 of 53 sites. However, this was not true for sites in Australia, where the retrieval accuracy of MODIS/Aqua AOD data was found to be poor due to the very low aerosol loading (monthly median AOD < 0.15) and the relatively higher surface reflectance of bare soil and/or desert. Disagreement in the AOD trends between MODIS and AERONET was also found at a few sites in South America. This was due to the low retrieval quality in MODIS/Aqua AOD and likely resulted from improper surface reflectance parameterization and uncertainties in the aerosol model used in the algorithm (Levy et al., 2010). Furthermore, sampling issues should be evaluated carefully when deriving long-term trends in AOD in regions where AOD shows substantial day-to-day variation.

Merged data based on the MODIS AOD products derived from both the DT and DB algorithms are used in many studies to investigate the long-term AOD trends over land areas in various locations throughout the world. In some regions, the typical AOD and its variability are low, close to the magnitude of the retrieval uncertainty, which affects the estimation of the AOD trends. However, the current MODIS AOD products do provide a continuous aerosol data record for monitoring long-term climate change.

Acknowledgements. This work was supported by the National Natural Science Foundation of China (Grant Nos. 41475027,

41475138 and 41675033). We are grateful to the AERONET team and MAPSS team, especially the PIs of the selected AERONET sites, for providing the data used in this study. We are also thankful for the suggestions and comments from the two anonymous reviewers and the editor, which helped to improve the manuscript.

REFERENCES

Boucher, O., and Coauthors, 2013: Clouds and Aerosols. *Climate Change 2013: The Physical Science Basis. Contribution of Working Group I to the Fifth Assessment Report of the Intergovernmental Panel on Climate Change*, T. F. Stocker et al., Eds., Cambridge University Press.

Chin, M., and Coauthor, 2014: Multi-decadal aerosol variations from 1980 to 2009: A perspective from observations and a global model. *Atmospheric Chemistry and Physics*, **14**, 3657–3690, https://doi.org/10.5194/acp-14-3657-2014.

de Meij, A., A. Pozzer, and J. Lelieveld, 2012a: Trend analysis in aerosol optical depths and pollutant emission estimates between 2000 and 2009. *Atmos. Environ.*, **51**, 75–85, https://doi.org/10.1016/j.atmosenv.2012.01.059.

de Meij, A., A. Pozzer, A., K. Pringle, H. Tost, and J. Lelieveld, 2012b: EMAC model evaluation and analysis of atmospheric aerosol properties and distribution with a focus on the Mediterranean region. *Atmos. Res.*, **114–115**, 38–69, https://doi.org/10.1016/j.atmosres.2012.05.014.

Hirsch, R. M., and J. R. Slack, 1984: A nonparametric trend test for seasonal data with serial dependence. *Water Res. Res.*, **20**, 727–732, https://doi.org/10.1029/WR020i006p00727.

Holben, B. N., and Coauthors, 1998: AERONET—A federated instrument network and data archive for aerosol characterization. *Remote Sens. Environ.*, **66**, 1–16, https://doi.org/10.1016/S0034-4257(98)00031-5.

Hsu, N. C., R. Gautam, A. M. Sayer, C. Bettenhausen, C. Li, M. J. Jeong, S. -C. Tsay, and B. N. Holben, 2012: Global and regional trends of aerosol optical depth over land and ocean using SeaWiFS measurements from 1997 to 2010. *Atmos. Chem. Phys.*, **12**, 8037–8053, https://doi.org/10.5194/acp-12-8037-2012.

Kahn, R. A., M. J. Garay, D. L. Nelson, K. K. Yau, M. A. Bull, B. J. Gaitley, J. V. Martonchik, and R. C. Levy, 2007: Satellite-derived aerosol optical depth over dark water from MISR and MODIS: Comparisons with AERONET and implications for climatological studies. *J. Geophys. Res.*, **112**, D18205, https://doi.org/10.1029/2006JD008175.

Kaufman, Y. J., B. N. Holben, D. Tanré, I. Slutsker, A. Smirnov, and T. F. Eck, 2000: Will aerosol measurements from Terra and Aqua Polar Orbiting satellites represent the daily aerosol abundance and properties? *Geophys. Res. Lett.*, **27**(23), 3861–3864.

Kokhanovsky, A. A., and Coauthors, 2007: Aerosol remote sensing over land: A comparison of satellite retrievals using different algorithms and instruments. *Atmos. Res.*, **85**, 372–394, https://doi.org/10.1016/j.atmosres.2007.02.008.

Levy, R. C., L. A. Remer, R. G. Kleidman, S. Mattoo, C. Ichoku, R. Kahn, and T. F. Eck, 2010: Global evaluation of the collection 5 MODIS dark-target aerosol products over land. *Atmos. Chem. Phys.*, **10**, 10 399–10 420, https://doi.org/10.5194/acp-10-10399-2010.

Levy, R. C., S. Mattoo, L. A. Munchak, L. A. Remer, A. M. Sayer, F. Patadia, and N. C. Hsu, 2013: The Collection 6 MODIS aerosol products over land and ocean. *Atmospheric Measurement Techniques*, **6**, 2989–3034, https://doi.org/10.5194/amt-6-2989-2013.

Li, Z., and Coauthors, 2009: Uncertainties in satellite remote sensing of aerosols and impact on monitoring its long-term trend: A review and perspective. *Ann. Geophys.*, **27**, 2755–2770, https://doi.org/10.5194/angeo-27-2755-2009.

Li, J., B. E. Carlson, O. Dubovik, and A. A. Lacis, 2014: Recent trends in aerosol optical properties derived from AERONET measurements. *Atmos. Chem. Phys.*, **14**, 12 271–12 289, https://doi.org/10.5194/acp-15-1599-2015.

Lyapustin, A., and Coauthors, 2014: Scientific impact of MODIS C5 calibration degradation and C6+ improvements. *Atmospheric Measurement Techniques*, **7**, 4353–4365, https://doi.org/10.5194/amt-7-4353-2014.

Mishchenko, M. I., I. V. Geogdzhayev, W. B. Rossow, B. Cairns, B. E. Carlson, A. A. Lacis, L. Liu, and L. D. Travis, 2007: Long-term satellite record reveals likely recent aerosol trend. *Science*, **315**, 1543, https://doi.org/10.1126/science.1136709.

Mishchenko, M. I., L. Liu, I. V. Geogdzhayev, J. Li, B. E. Carlson, A. A. Lacis, B. Cairns, and L. D. Travis, 2012: Aerosol retrievals from channel-1 and -2 AVHRR radiances: Long-term trends updated and revisited. *Journal of Quantitative Spectroscopy and Radiative Transfer*, **113**, 1974–1980, https://doi.org/10.1016/j.jqsrt.2012.05.006.

Petrenko, M., C. Ichoku, and G. Leptoukh, 2012: Multi-sensor Aerosol Products Sampling System (MAPSS). *Atmospheric Measurement Techniques*, **5**, 913–926, https://doi.org/10.5194/amt-5-913-2012.

Pozzer, A., A. de Meij, J. Yoon, H. Tost, A. K. Georgoulias, and M. Astitha, 2015: AOD trends during 2001–2010 from observations and model simulations. *Atmos. Chem. Phys.*, **15**, 5521–5535, https://doi.org/10.5194/acp-15-5521-2015.

Qin, Y., and R. M. Mitchell, 2009: Characterisation of episodic aerosol types over the Australian continent. *Atmospheric Chemistry and Physics*, **9**, 1943–1956, https://doi.org/10.5194/acp-9-1943-2009.

Sayer, A. M., N. C. Hsu, C. Bettenhausen, and M. -J. Jeong, 2013: Validation and uncertainty estimates for MODIS Collection 6 "Deep Blue" aerosol data. *J. Geophys. Res.*, **118**, 7864–7872, https://doi.org/10.1002/jgrd.50600.

Sen, P. K., 1968: Estimates of the regression coefficient based on Kendall's tau. *Journal of the American Statistical Association*, **63**, 1379–1389, https://doi.org/10.1080/01621459.1968.10480934.

Thomas, G. E., and Coauthors, 2010: Validation of the GRAPE single view aerosol retrieval for ATSR-2 and insights into the long term global AOD trend over the ocean. *Atmos. Chem. Phys.*, **10**, 4849–4866, https://doi.org/10.5194/acp-10-4849-2010.

Xia, X. G., 2011: Variability of aerosol optical depth and Ångström wavelength exponent derived from AERONET observations in recent decades. *Environ. Res. Lett.*, **6**, 044011, https://doi.org/10.1088/1748-9326/6/4/044011.

Yue, S., and C. Y. Wang, 2002: Applicability of prewhitening to eliminate the influence of serial correlation on the Mann-Kendall test. *Water Resour. Res.*, **38**(6), 1068, https://doi.org/10.1029/2001WR000861.

Yue, S., P. Pilon, B. Phinney, and G. Cavadias, 2002: The influence of autocorrelation on the ability to detect trend in hydrological series. *Hydrological Processes*, **16**, 1807–1829.

Yoon, J., W. von Hoyningen-Huene, M. Vountas, and J. P. Burrows,

2011: Analysis of linear long-term trend of aerosol optical thickness derived from SeaWiFS using BAER over Europe and South China. *Atmos. Chem. Phys.*, **11**, 12 149–12 167, https://doi.org/10.5194/acp-11-12149-2011.

Yoon, J., W. von Hoyningen-Huene, A. A. Kokhanovsky, M. Vountas, and J. P. Burrows, 2012: Trend analysis of aerosol optical thickness and Ångström exponent derived from the global AERONET spectral observations. *Atmospheric Measurement Techniques*, **5**, 1271–1299, https://doi.org/10.5194/amt-5-1271-2012.

Yu, H., M. Chin, L. A. Remer, R. G. Kleidman, N. Bellouin, H. Bian, and T. Diehl, 2009: Variability of marine aerosol fine mode fraction and estimates of anthropogenic aerosol component over cloud-free oceans from the Moderate resolution Imaging Spectroradiometer (MODIS). *J. Geophys. Res.*, **114**, D10206, https://doi.org/10.1029/2008JD010648.

Zhang, J., and J. S. Reid, 2010: A decadal regional and global trend analysis of the aerosol optical depth using a data-assimilation grade over-water MODIS and Level 2 MISR aerosol products. *Atmos. Chem. Phys.*, **10**, 10 949–10 963, https://doi.org/10.5194/acp-10-10949-2010.

Zhang, J. L., J. S. Reid, R. Alfaro-Contreras, and P. Xian, 2017: Has China been exporting less particulate air pollution over the past decade? *Geophys. Res. Lett.*, **44**, 2941–2948, https://doi.org/10.1002/2017GL072617.

Zhao, X.-P., I. Laszlo, W. Guo, A. Heidinger, C. Cao, A. Jelenak, D. Tarpley, and J. Sullivan, 2008: Study of long-term trend in aerosol optical thickness observed from operational AVHRR satellite instrument. *J. Geophys. Res.*, **113**, D07201, https://doi.org/10.1029/2007JD009061.